Catal Lett (2009) 129:513–518
DOI 10.1007/s10562-008-9834-5

Synthesis, Characterization of Fe-doped TiO_2 Nanotubes with High Photocatalytic Activity

Lixue Deng · Shurong Wang · Daying Liu · Baolin Zhu · Weiping Huang · Shihua Wu · Shoumin Zhang

Received: 17 October 2008 / Accepted: 25 December 2008 / Published online: 30 January 2009

Abstract Fe-doped titanate nanotubes were prepared by the combination of sol–gel process with hydrothermal treatment. After a further calcinations process, Fe-doped TiO_2 nanotubes (Fe/TiO_2 NTs) with high photocatalytic activity were obtained. The prepared catalysts were characterized by XRD, TEM, and XPS. The photocatlytic activity of Fe/TiO_2 NTs was evaluated through the photodegradation of aqueous methyl orange. The experiments demonstrated that the 0.5% Fe/TiO_2 NTs calcined at 300 °C possessed the best photocatalytic activity. Compared with pure TiO_2 nanotubes, the doping with Fe significantly enhanced the photocatalytic efficiency.

Keywords Titanium dioxide · Nanotubes · Doping · Iron ions · Photocatalytic activity

1 Introduction

Semiconductor photocatalysis is a promising technology in air purification, water disinfection, hazardous waste remediation, and water purification. Several semiconductors have band gap energies sufficient for promoting or catalyzing a wide range of chemical reactions of environmental interest [1]. Among various candidates, TiO_2 is proved to be the most suitable catalyst for widespread environmental applications because of its biological and chemical properties and cost-effectiveness [2, 3]. However, titanium dioxide is limited in practical applications for its low photoefficiency in photocatalytic reaction and weak photoresponse in visible range. Doping with suitable transitional metals has been attempted to improve its performances [4, 5]. Because the radius of Fe^{3+} is close to that of Ti^{4+}, special efforts have been dedicated to doping TiO_2 with Fe [6–17]. It has been reported that Fe ions can act as shallow charge traps in the TiO_2 lattice and result in high photocatalytic activity [1, 18].

Recently, extensive researches have been conducted on the synthesis and characterization of TiO_2 nanotubes (TiO_2 NTs) because of their novel properties, such as unique shape, size confinement in radial-direction and large specific surface area [19–24]. Furthermore, the high sedimentation rate of the nanotubes facilitate their reuse as photocatalystes [25]. However, their relatively low photocatalytic activity still restricts their application. We have reported that the doping of TiO_2 NTs with Cr significantly enhanced the photocatalytic activity for the photodegradation of *p*-nitroaniline [26]. Xu et al. have reported the preparation of zinc surface-doped TiO_2 NTs [27]. Compared with TiO_2 NTs, the Zn-doped TiO_2 NTs showed higher photocatalytic activity. There are several papers about Fe-doped titanate nanotubes. Titanate nanotubes have been prepared by Song et al. [28, 29]. Ding and Xu et al. have prepared Fe-incorporated titanate nanotubes, and investigated their electronic, optical, and magnetic properties [30–32]. Chang et al. have prepared Fe^{3+}-substituted titanate nanotubes by alkali hydrothermal method using Fe^{3+}-doped rutile TiO_2 nanopowders as precursors [33]. The titanate nanotubes possessed the crystalline orthorhombic system, and had the best photocatalytic activity for degradation of Rhodamine B when the Fe^{3+} doping concentration was 2.0%. Han et al. have synthesized Fe-doped trititanate nanotubes, and the nanotubes exhibited noticeable catalytic activity in the water-gas-shift reaction [34]. Compared with Fe-doped titanate nanotubes, higher

L. Deng · S. Wang · D. Liu · B. Zhu · W. Huang · S. Wu · S. Zhang (✉)
Department of Chemistry, Nankai University, Tianjin 300071, China
e-mail: zhangsm@nankai.edu.cn

photocatalytic activity can be expected on anatase Fe/TiO_2 NTs.

However, to our knowledge, photocatalysis upon anatase Fe/TiO_2 NTs have not been reported. In this paper, Fe/TiO_2 NTs were prepared by using Fe-doped anatase TiO_2 nanopowders as precursors. The products were characterized by XRD, TEM, and XPS. Their photocatalytic activity under UV-vis light irradiation was evaluated by the degradation of methyl orange.

2 Experimental

All the reagents were analytical grade and used without any further purification.

2.1 Preparation of Fe/TiO_2 NTs

The Fe-doped TiO_2 powder was prepared by the sol–gel route using tetrabutyl titanate and ferric nitrate as the precursors. Under constant stirring, ethanol solution of tetranbutyl titanate (ethanol versus tetranbutyl titanate volume ratio is 4:1) was added drop-wise to the mixture of 20 mL ethanol and 0.045 mol/L ferric nitrate solution. The transparent sol was obtained when the mixture was hydrolyzed at room temperature for 2 h under vigorous stirring. Then gel was obtained by aging the sol for 12 h at room temperature. The resulting gel was dried at 80 °C in oven for 12 h to remove the solvents and then calcined at 500 °C in muffle for 3 h. Then the Fe-doped TiO_2 powder was obtained. The calculated Fe concentration were 0.5, 0.75, 1.0%, respectively. Pure TiO_2 powder was synthesized with the same process except that distilled water instead of ferric nitrate solution is used. To obtain pure titanate nanotubes and doped nanotubes with different Fe concentration, 1.2 g Fe-doped TiO_2 powder or pure TiO_2 powder was mixed with 58 mL 10 mol/L NaOH aqueous solution in a Teflon vessel and maintained at 150 °C for 12 h. Obtained materials were washed with 0.1 mol/L HNO_3 solution and distilled water, respectively, and then dried at 80 °C overnight in oven. After the prepared material was calcined at different temperature for 2 h, Fe/TiO_2 NTs were obtained. The obtained corresponding concentrations photocatalysts were expressed as wt.%.

2.2 Samples Characterization

The powder X-ray diffraction (XRD) experiments were carried out at room temperature using a Rigaku D/Max-2500 X-ray diffractometer (CuKα $\lambda = 0.154$ nm) to identify crystal phase of the products. TEM images were obtained with a Philips T20ST transmission electron microscopy working at 200 kV. The charge state of doped TiO_2 at the surface was investigated by X-ray photoelectron spectroscopy (XPS) using an Al X-ray source (Al $K\alpha$-150 W, Kratos Axis Ultra DLD).

2.3 Photoactivity Measurement

The photocatalytic activity under UV-vis light irradiation of the prepared catalysts was evaluated by the degradation rates of methyl orange (20 mg/L) in an aqueous solution (100 mL) containing 50 mg of sample. The reaction mixture was ultrasonically dispersed for 30 min, and then irradiated by using a 300 W High-Pressure Mercury Lamp under stirring. The radiate range of the High-Pressure Mercury Lamp is from 200 nm to 1,000 nm, and the full spectrum of selected wavelength was used for experiments. After every given irradiation time, a sample of 5 mL suspension was withdrawn, centrifugated and filtered. The obtained solution was then measured for checking the residual concentration of methyl orange with a UV-vis spectrophotometer (TU-1901) at 463.8 nm, which is the maximum absorption of methyl orange. The results are corrected for the decomposition of methyl orange in the absence of catalysts and for absorption of methyl orange on the catalyst.

3 Results and Discussion

Figure 1 depicts the XRD patterns of 0.5% Fe-doped nanotube without calcination and calcined at different temperatures. Diffractions that are attributable to anatase TiO_2 are clearly detectable in the calcinated materials (JCPDS 21-1272). For the sample without calcination, the peak at $2\theta = 25.3°$ is asymmetric, one shoulder peak at

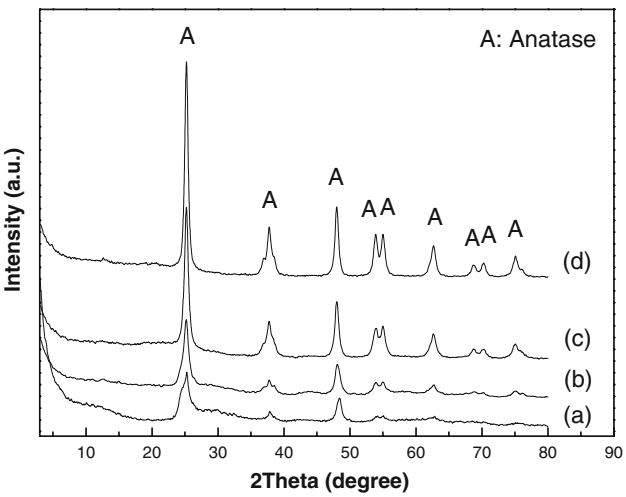

Fig. 1 XRD patterns of 0.5% Fe-doped nanotubes without calcination (**a**) and calcined at 200 °C (**b**); 300 °C (**c**); 400 °C (**d**)

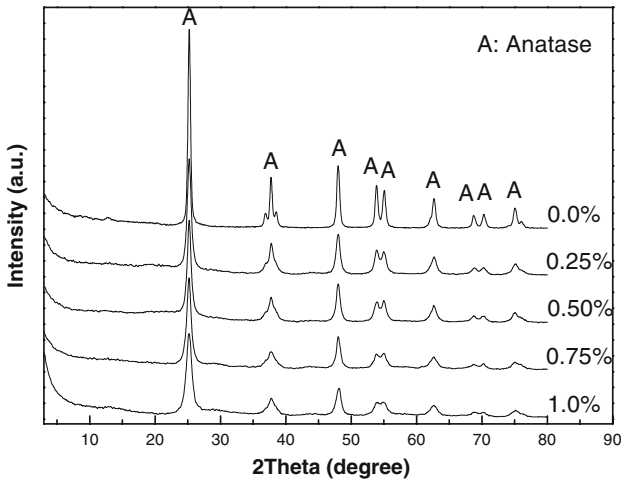

Fig. 2 XRD patterns of Fe/TiO_2 NTs calcined at 300 °C with various Fe doping concentration

lower 2θ can be identified, which implies the existence of titanate [22, 23, 26]. However, the peak of titanate is not present in the calcined nanotubes, which indicates that titanate decomposes into pure anatase TiO_2 by calcination treatment [24, 26, 35]. The width of all reflection lines is decreased with increasing calcination temperatures without a change in the overall patterns of the diffraction lines, which is attributed to the enhancement of crystallinity with increasing calcination temperatures.

Figure 2 shows XRD patterns of Fe/TiO_2 NTs calcined at 300 °C with various Fe doping concentration. Within the detection limits of this technique, all samples consist of anatase as the unique phase. However, no crystalline phase containing Fe could be observed, even at the highest Fe concentration. It indicates that the iron ions are highly dispersed on TiO_2, and XRD is not sensitive enough to detect such minor changes to TiO_2. Compared to TiO_2 NTs, the pattern peaks for Fe/TiO_2 NTs are slightly weaken and broaden. Since the radius of Fe^{3+} is 0.64 Å, which is a little smaller than 0.77 Å channels along the *c*-axis in TiO_2 NTs and close to the radius of Ti^{4+} (0.68 Å), it is possible that Fe^{3+} diffuses along the *c*-axis and substitutes Ti^{4+} in the TiO_2 lattice. Due to the different atomic sizes of Fe^{3+} and Ti^{4+}, some extent of deformation is introduced into the crystal lattice of TiO_2 [36]. Such a substitution not only lowers the crystallization of TiO_2, which is reflected by a weaker diffraction intensity of XRD pattern, but also slightly restrains the growth of TiO_2 crystallite. As a result of dopant substitution, similar phenomena have also been observed in other transitional metal doping systems [37].

Figure 3 shows TEM images of 0.5% Fe-doped nanotubes. Nanotubular structures are clearly observed in both of them. Figure 3a and b indicate that the obtained nanotubes are hollow and open-ended. Their diameters are nearly uniform and their length is more than hundreds of nanometers, similar to the results reported by Kasuga [19, 20]. The nanotube structure has an outer diameter of about 10 nm. Figure 3c shows the TEM image of Fe/TiO_2 NTs calined at 300 °C. It can be seen that most of the nanotubes keep their tubular texture after the calcination process. Figure 3d shows a cross-sectional image of two nanotubes. It can be inferred from this image that Fe/TiO_2 NTs are formed by rolling up the anatase single-layer sheets. This explains why the walls viewed on the two sides of Fe/TiO_2 NTs are generally unequal [19, 21].

Figure 4a shows the XPS survey spectra of Fe/TiO_2 NTs calcined at 300 °C. There are Ti, O, Fe, and C on the surface of Fe-doped TiO_2. The C 1s peak is at 285.8 eV. The residual carbon resulted from the organic precursors used in the sol–gel method. The adventitious hydrocarbon from XPS itself may also cause the presence of C element. The doping concentration of Fe analyzed by XPS is 3.3%. The actual content of Fe dopant is examined to be 0.4% by ICP measurement, which is some less than the nominal values in Fe doped samples. It should be attributed to the incomplete doping of Fe ion, which is confirmed by checking out a little amount of Fe^{3+} ion in the filtrate after the hydrothermal doping treatment. However, the surface Fe content determined by XPS is much higher than the total Fe content measured by ICP, which implies that Fe dopant has a much higher concentration at the exterior than that at the interior of TiO_2. The work mechanism of hydrothermal doping treatment may be the reason for the above result. In this process, Fe^{3+} ions firstly adsorbed mostly and strongly on the surface of TiO_2 gel due to its high surface area and strong electrostatic interaction. Then the Fe^{3+} ions diffuse gradually into the bulk of TiO_2 grains by injecting into the Ti^{4+} vacancy or substituting Ti^{4+} ions in crystallization of TiO_2 during the long-time hydrothermal treatment, since the crystalline structure of TiO_2 are in great change under the hydrothermal condition. Therefore, the content of Fe^{3+} decreases in the direction of the diffusion, from the exterior to the interior [37].

Figure 4b shows the high resolution XPS spectra of Ti 2p. The Ti $2p_{1/2}$ and Ti $2p_{3/2}$ spin-orbital splitting photoelectrons are located at binding energies of 464.1 and 458.3 eV, respectively, which was in agreement with the reported literature values [38, 39], showing the presence of Ti^{4+}. Figure 4c shows the O 1s XPS spectra of Fe/TiO_2 NTs. The O 1s spectrum was asymmetric. The main peak of O 1s located at about 530.8 eV is at a similar energy to the O 1s electron binding energy for TiO_2, corresponding to lattice oxygen of TiO_2. The O 1s signal showed a shoulder located at the side of higher binding energies, indicating a great amount of surface hydroxyl groups or chemisorbed water molecules [38, 39].

Figure 4d Fe-doped trititanate nanotubes, shows the higher solution XPS spectra of the Fe $2p_{3/2}$ region of

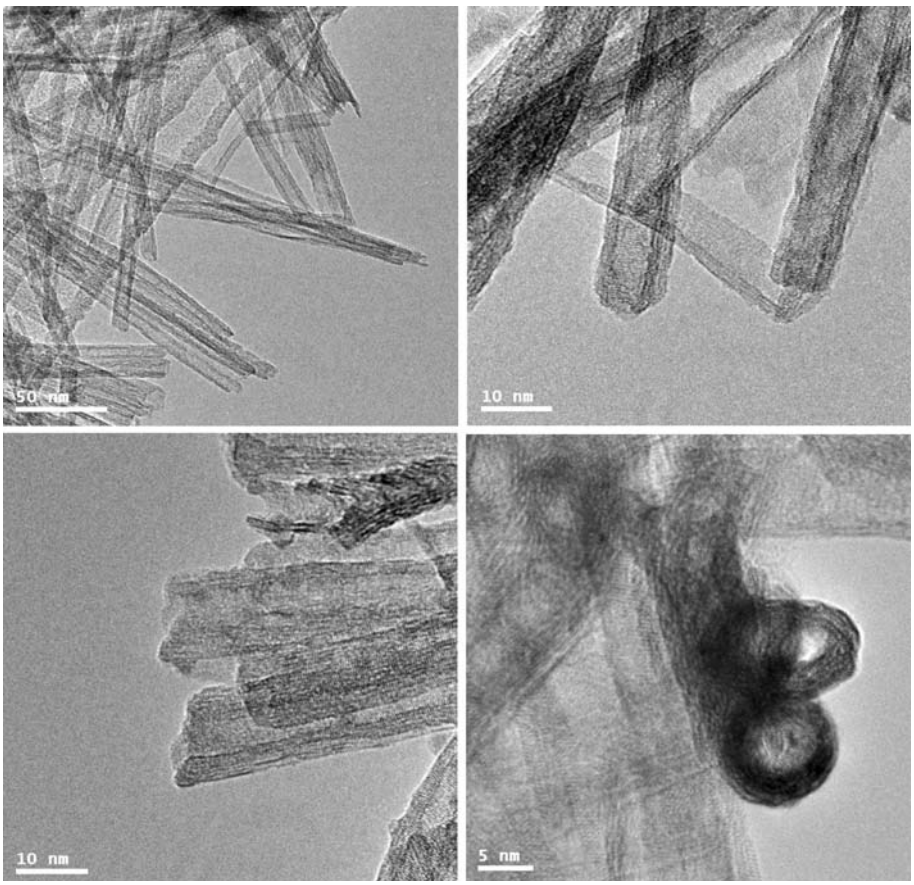

Fig. 3 TEM images of 0.5% Fe-doped nanotube without calcination (**a**, **b**), calcined at 300 °C (**c**), and cross-sectional view (**d**)

Fe/TiO_2 NTs. The signals of Fe are very weak, due to the low doping level. The binding energies at around 712.3 and 710.6 eV should be assigned to Fe^{3+} $2p_{3/2}$ and Fe^{2+} $2p_{3/2}$, respectively. The formation of Fe^{2+} ions could be ascribed to the presence of residual carbon in the films from organic radicals introduced by precursors. During thermal treatment, the oxidation of carbon would draw oxygen from the surrounding atmosphere and TiO_2 network, resulting in the reduction of Fe^{3+} to Fe^{2+} [14, 40].

Figure 5 shows the degradation rates of methy orange for pure TiO_2 powder and pure TiO_2 nanotube calcined at 300 °C for 2 h. About 69.1% of the methyl orange is degraded after 3 h irradiation in the presence of pure TiO_2 powder, while 63.5% of the methyl orange is degraded in the presence of pure TiO_2 nanotube. Obviously, the photocatalytic activity of the pure TiO_2 nanotube is better than that of pure TiO_2 powder. TiO_2 nanotubes (TiO_2 NTs) have novel properties, such as unique shape, size confinement in radial-direction and large specific surface area. The special structure of the nanotubes will result in improved adsorptive ability and better photocatalytic activity can be obtained.

Calcination is an effective treatment method to enhance the photocatalytic activity of Fe-doped nanotubes. As shown in Fig. 6, 14.5, 64.6, 99.7, and 80.6% of the methyl orange is degraded after 3 h irradiation in the presence of Fe-doped nanotubes without calcination, calcined at 200, 300, and 400 °C, respectively. It is obviously that the doped nanotubes without calcination show much low photocatalytic activity. This was attributed to the existence of titanate. When calcined at 200 °C, Fe/TiO_2 NTs show obvious photocatalytic activity due to the formation of anatase. It has been generally accepted that anatase TiO_2 works better during the photocatalytic process. After the calcination treatment, titanate turn into anatase TiO_2 and higher photocatalytic activity is obtained. From Fig. 1, it can be seen that the content of anatase TiO_2 increased with the increase of calcination temperature. The Fe-doped TiO_2 nanotubes calcined at 300 °C possess the best photocatalytic activity. This result is also in accordance with the result that is reported by Zhang et al. [24]. They reported that regarding the photo-degradation of propylene, TiO_2 nanotubes treated at 300 °C possess the best photocatalytic ability among the thermally treated TiO_2 nanotubes. The photocatalytic activity of Fe/TiO_2 NTs decreases with a further increase in calcination temperature (Fig. 6d). That is probably due to the agglomeration and sintering damage of nanotubes caused by calcination at high temperature [27].

Figure 7 shows the photodegradation of methyl orange for Fe/TiO_2 NTs as a function of Fe doping concentration. All the catalysts were calcined at 300 °C. About 69.1, 70.7,

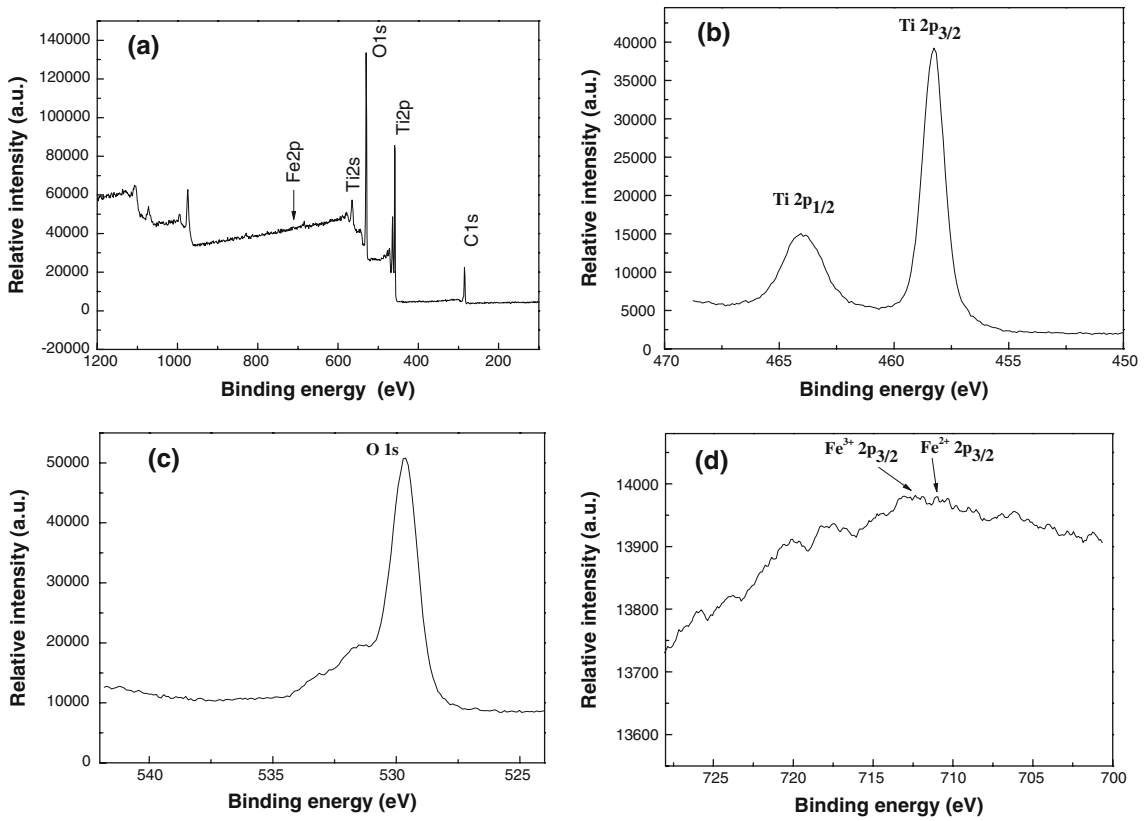

Fig. 4 XPS spectra of 0.5% Fe/TiO_2 NTs: **a** survey; **b** Ti 2p peaks; **c** O 1s peaks; and **d** Fe 2p peaks

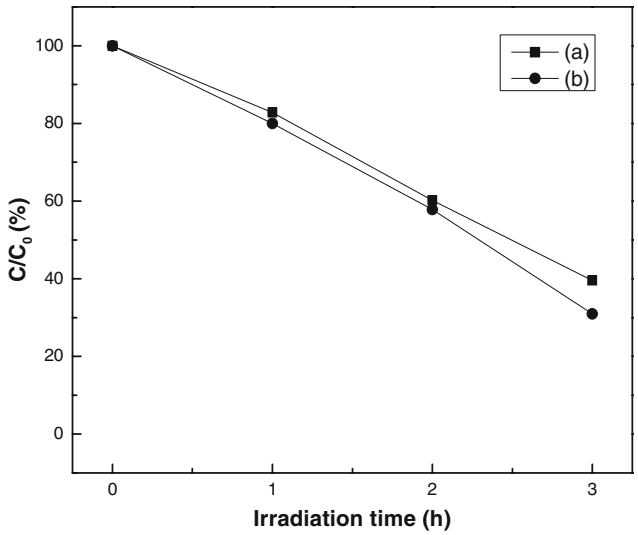

Fig. 5 Photocatalytic activity of pure pure TiO_2 powder (**a**) and pure TiO_2 nanotube (**b**)

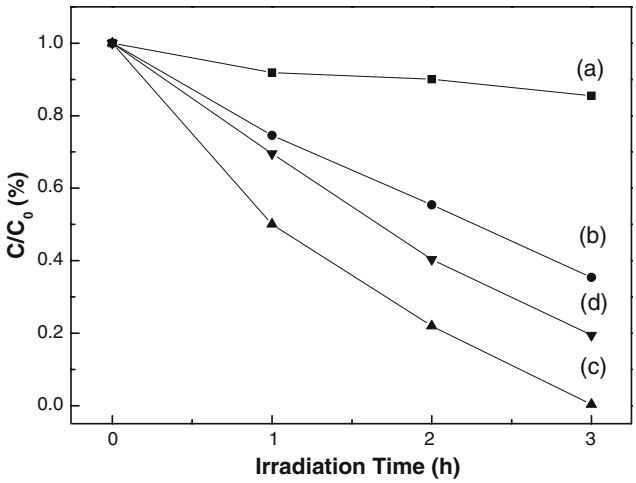

Fig. 6 Photodegradation of methyl orange by 0.5% Fe-doped nanotube without calcination (**a**) and calcined at 200 °C (**b**); 300 °C (**c**); 400 °C (**d**)

99.7, 62.8, 40.4% of the methyl orange is degraded after 3 h irradiation in the presence of TiO_2 NTs with 0, 0.25, 0.5, 0.75, and 1.0% Fe doping, respectively.

The results reveal that the photocatalytic performance of TiO_2 NTs can be improved by the doping of iron ions. This may be due to the fact that a small amount of Fe^{3+} ions can act as a photo-generated hole and a photo-generated electron trap and inhibit the hole–electron recombination [4, 6]. Detrapping and/or transfer of trapped charges to the interface to initiate the photoreactions must also be efficient processes. In Fe-doped samples, electrons are either directly trapped at Ti(IV) surface sites (form Ti^{3+}) or in deeper Fe(III) sites (form Fe^{2+}). In this case, the trapped

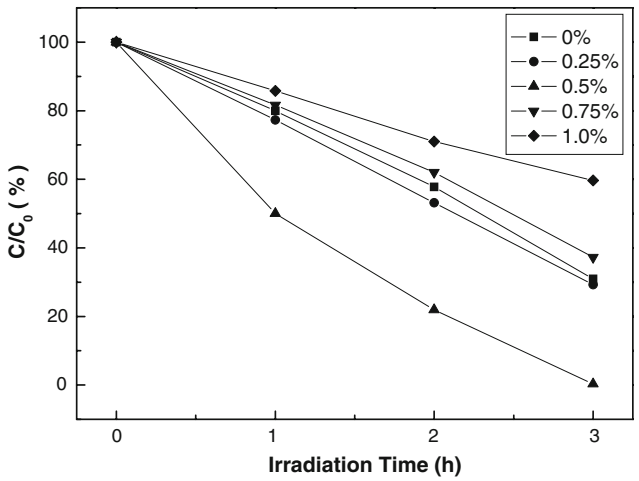

Fig. 7 Effect of photodegradation of methyl orange on Fe/TiO_2 NTs with various Fe doping concentration

electron can be easily transferred from Fe^{2+} to a neighboring surface Ti^{4+} because of the proximity of the energy levels [4]. As a result, the photocatalytic activity is improved after the Fe doping. Furthermore, high catalytic activity for the Fe-doped samples under visible light is expected, and this research work is under further investigation.

4 Conclusions

Fe-doped titanate nanotubes are prepared by the combination of sol–gel process with hydrothermal treatment. After a further calcination, the titanate decomposes to anatase TiO_2, and Fe/TiO_2 NTs are obtained as a result. Fe substitution not only lowers the crystallization of TiO_2 but also slightly restrains the growth of TiO_2 crystallite. The nanotubes are hollow and open-ended, and their length is more than hundreds of nanometers. Most of the nanotubes keep their tubular texture after the calcination process. The 0.5% Fe/TiO_2 NTs calcined at 300 °C possess the best photocatalytic activity.

Acknowlegments This work was supported by the National Natural Science Foundation of China (Grant No. 20771061) and 973 Program (2005CB623607).

References

1. Hoffmann MR, Martin ST, Choi W, Bahnemannt DW (1995) Chem Rev 95:69
2. Linsebigler AL, Lu GQ, Yates JT (1995) Chem Rev 95:735
3. Fujishima A, Rao TN, Tryk DA (2000) J Photochem Photobiol C 1:1
4. Choi W, Termin A, Hoffmann MR (1994) J Phys Chem 98:13669
5. Litter MI (1999) Appl Catal B 23:89
6. Litter MI, Navío JA (1996) J Photochem Photobiol A 98:171
7. Navío JA, Colón G, Macías M, Real C, Litter MI (1999) Appl Catal A 177:111
8. Navío JA, Testa JJ, Djedjeian P, Padrón JR, Rodríguezb D, Litter MI (1999) Appl Catal A 178:191
9. Dhananjeyan MR, Kandavelu V, Renganathan R (2000) J Mol Catal A 151:217
10. Li XY, Yue PL, Kutal C (2003) New J Chem 27:1264
11. Yu JC, Ho W, Lin J, Yip H, Wong PK (2003) Environ Sci Technol 37:2296
12. Kim DH, Hong HS, Kim HJ, Song JS, Lee KS (2004) J Alloys Compd 375:259
13. Kumbhar A, Chumanov G (2005) J Nanopart Res 7:489
14. Zhou MH, Yu JG, Cheng B, Yu HG (2005) Mater Chem Phys 93:159
15. Wang XH, Li JG, Kamiyama H, Moriyoshi Y, Ishigaki T (2006) J Phys Chem B 110:6804
16. Zhu JF, Chen F, Zhang JL, Chen HJ, Anpo M (2006) J Photochem Photobiol A 180:196
17. Adán C, Bahamonde A, Fernández-García M, Martínez-Arias A (2007) Appl Catal B 72:11
18. Piera E, Tejedor-Tejedor MI, Zorn ME, Anderson MA (2003) Appl Catal B 46:671
19. Kasuga T, Hiramatsu M, Hoson A, Sekino T, Niihara K (1998) Langmuir 14:3160
20. Kasuga T, Hiramatsu M, Hoson A, Sekino T, Niihara K (1999) Adv Mater 11:1307
21. Yao BD, Chan YF, Zhang XY, Zhang WF, Yang ZY, Wang N (2003) Appl Phys Lett 82:281
22. Yang JJ, Jin ZS, Wang XD, Li W, Zhang JW, Zhang SL, Guo XY, Zhang ZJ (2003) Dalton Trans 20:3898
23. Bavykin DV, Parmon VN, Lapkin AA, Walsh FC (2004) J Mater Chem 14:3370
24. Zhang M, Jin ZS, Zhang JW, Guo XY, Yang JJ, Li W, Wang XD, Zhang ZJ (2004) J Mol Catal A 217:203
25. Li H, Zhu BL, Feng YF, Wang SR, Zhang SM, Huang WP (2007) J Solid State Chem 180:2136
26. Zhang SM, Chen YY, Yu Y, Wu HH, Wang SR, Zhu BL, Huang WP, Wu SH (2008) J Nanopart Res 10:871
27. Xu JC, Lu M, Guo XY, Li HL (2005) J Mol Catal A 226:123
28. Song XC, Yue LH, Liu B, Han G, Chen WX, Xu ZD (2003) Chin J Inorg Chem 19:899
29. Song XC, Zheng YF, Cao GS, Yin HY (2005) Chin J Inorg Chem 21:1897
30. Ding X, Xu XG, Chen Q, Peng LM (2006) Nanotechnology 17:423
31. Xu XG, Ding X, Chen Q, Peng LM (2006) Phys Rev B 73: 165403/1
32. Xu XG, Ding X, Chen Q, Peng LM (2007) Phys Rev B 75: 035423/1
33. Chang XF, Liu ZH, Li C, Yang GF, Jia LP (2007) Nanoscience 12:25
34. Han WQ, Wen W, Yi D, Liu ZX, Maye MM, Lewis L, Hanson J, Gang O (2007) J Phys Chem C 111:14339
35. Zhu BL, Sui ZM, Wang SR, Chen X, Zhang SM, Wu SH, Huang WP (2006) Mater Res Bull 41:1097
36. Wang ZM, Yang G, Biswas P, Bresser W, Boolchand P (2001) Powder Technol 114:197
37. Zhu J, Deng Z, Chen F, Zhang J, Chen H, Anpo M, Huang J, Zhang L (2006) Appl Catal B 62:329
38. Liu HM, Yang WS, Ma Y, Cao YA, Yao JN, Zhang J, Hu TD (2003) Langmuir 19:3001
39. Nagaveni K, Hegde MS, Ravishankar N, Subbanna GN, Madras G (2004) Langmuir 20:2900
40. Zhou MH, Yu JG, Cheng B (2006) J Hazard Mater B 137:1838